AGU PUBLICATIONS

JGR

Journal of Geophysical Research: Oceans

RESEARCH ARTICLE

10.1002/2014JC009896

Key Points:
- Characterization of dissipation rates for swells
- Dissipation induced by turbulent atmospheric shear stress

Correspondence to:
Y. Perignon,
yves.perignon@ec-nantes.fr

Citation:
Perignon, Y., F. Ardhuin, M. Cathelain, and M. Robert (2014), Swell dissipation by induced atmospheric shear stress, *J. Geophys. Res. Oceans*, *119*, 6622–6630, doi:10.1002/2014JC009896.

Received 10 FEB 2014
Accepted 9 SEP 2014
Accepted article online 15 SEP 2014
Published online 6 OCT 2014

Swell dissipation by induced atmospheric shear stress

Y. Perignon[1], F. Ardhuin[2], M. Cathelain[1], and M. Robert[1]

[1]Ecole Centrale de Nantes, Laboratoire d'Hydrodynamique, Energétique et Environnement Atmosphérique, Nantes, France, [2]Ifremer, Laboratoire d'Océanographie Spatiale, Brest, France

Abstract Observations of swell dissipation across oceans reveal a significant loss of energy that can be the result of many of processes. Among these candidate mechanisms, this paper examines the properties of the viscous air-sea boundary layer driven by swells in order to characterize the induced atmospheric flow regime and its associated viscous dissipation over swells. A series of 3-D numerical experiments is carried out with a RANS model and appropriate turbulence closure. These experiments reveal a laminar to turbulent transition in the near free-surface region for a common range of characteristic amplitudes and periods of swells under stationary conditions. At low Reynolds number, laminar conditions prevail and computed decay rates conform to the analytical formulation μ_v of the Stokes interfacial boundary layer for this problem. The turbulent regimes are characterized as well, and the new decay rates follow a nondimensional relation $\mu = 1.42\mu_v \left(\frac{\mathrm{Re}}{1.5\times10^5}\right)^{0.41}$ above $\mathrm{Re} = 1.5\times10^5$ (e.g., amplitude larger than 1.1 m for a 14 s monochromatic wave period). Typical decay rates are up to 4 times above the laminar values, which is a factor 10 less than the largest rates estimated for oceanic conditions. A sensitivity analysis is finally conducted to evaluate the influence of the stationary hypothesis. It demonstrates a short setup length and low relative variations of the unsteady decay rates for laminar, transitioning and developed turbulent conditions, which confirms the evaluation of steady decay rates.

1. Introduction

Swells are commonly defined as surface wave following propagation paths out of reach of their originated wind. Swells often radiate across ocean basins and can carry out a significant and persistent amount of energy over several thousand kilometers from their source. Still, global observations of ocean swells from satellite data have revealed that a significant energetic loss occurs, proportionally more so for steeper swells [*Ardhuin et al.*, 2009]. Many processes are still candidate to this date for the closure of the energy balance along its propagation path. These include the interaction of swell with oceanic turbulence [see e.g., *Phillips*, 1961; *Guo and Shen*, 2013] or with the atmosphere coupling [e.g., *Harris*, 1966].

We present in this paper, a study on the latter mechanism neglecting for now any interaction between the wave-induced flow and an atmospheric-driven flow (i.e., no mean wind). The retroaction of the atmospheric shear stress induced by swell remains poorly quantified, and more particularly when water orbital velocity and particle displacement reach a turbulent threshold for the motion they impose in the air side [*Collard et al.*, 2009]. The characterization of this turbulent flow regime and magnitude of its induced dissipation over the underlying swell remain a major question to address. When neglecting the surface curvature, one can recover the known viscous results of an oscillatory boundary layer over a fixed bottom [see *Gundogdu and Carpinlioglu*, 1999a, 1999b for a detailed review of this subbranch class of the general problem of boundary layer in pulsatile flows]. For an extensive analysis of the flow with account of the wave properties (i.e., wave length, and to a lower extent surface curvature), the lack of experimental evidence can easily be related to the complex setup required by field measurements, as well as laboratory experiments [e.g., *Young and Sobey*, 1985]. Indeed, the atmospheric boundary layer of characteristic thickness $\delta = \sqrt{2\nu/\omega} \equiv O(10^{-3}\mathrm{m})$ needs to be qualified along a wavelength $O(100\,\mathrm{m})$ in a frame of vertical displacement $O(1\,\mathrm{m})$. In order to investigate the laminar to turbulent dynamics of this boundary layer, numerical experiments are conducted using the computational fluid dynamics (CFD) software STAR-CCM+ [*STAR-CCM+*, 2013]. The evolution of the shear is reviewed for a wide range of swell conditions and enables to quantify the expected turbulent increase in work and associated dissipation rates at free surface.

Section 2 of this paper details the general framework of the problem and recalls its analytical resolution under the assumption of low steepness for the ongoing swell [*Dore*, 1978; *Weber*, 1983]. Section 3 describes the setup of the series of numerical experiments and the model for the air-sea interface implemented with CFD. Section 4.1 presents the results of the numerical experiment under steady swell conditions. In section 4.2, the associated dissipation rates are evaluated and their evolution under the turbulent shear stress is quantified. A parameterization of the dissipation rate against a characteristic Reynolds number is proposed. Section 4.3 evaluates the sensitivity of the previous results to the hypothesis of steady swell conditions. Section 5 contains final discussions and conclusions of this work.

2. Theoretical Framework

When studying the problem of a swell propagating under a viscous atmospheric layer at initial rest, one can consider the ocean layer as a strong forcing toward the atmospheric layer, and the atmospheric flow as a weak forcing on the free surface. We propose here a study of the local strongly forced atmospheric flow so as to characterize a theoretical large-scale weak retroaction on an ideal swell. For the sake of simplicity, the swell cases will be considered as unidirectional and monochromatic waves.

A first characterization of the flow can be achieved following *Collard et al*. [2009], neglecting the curvature of the surface. One can recover a characteristic Reynolds number for the atmospheric flow, based on the double velocity and double displacement for an analogy with fixed bottom boundary layer problems, i.e.,

$$\mathrm{Re} = \frac{4u_{orb}a_{orb}}{\nu}. \tag{1}$$

For the monochromatic linear case, u_{orb} and a_{orb} correspond to the amplitude of the surface velocity u_- and displacement η.

The flow is expected to be turbulent above Re $\sim 10^5$ [*Jensen et al*., 1989] and the atmospheric shear stress at free surface to depart from the laminar analytical solution from *Dore* [1978]. The laminar solution is expressed as the sum of the potential flow theory and a viscous sublayer enabling to connect velocity profiles through both mediums. The viscous layer in water is neglected due to the higher water inertia and to the range of long waves considered here. For deepwater waves of linear profile, solution of the Euler equation, $\eta(x,t)=a\cos(kx-\omega t)$, the horizontal subsurface velocity is $u_-(x,t)=\omega a\cos(kx-\omega t)$, where $\omega=2\pi/T$ accounts for the angular frequency. The Euler solution for the atmospheric velocity profile verifies the same potential flow solution as the ocean side, with a connection to the ocean layer by a viscous boundary layer such as

$$u_+(x,z,t) = -\omega a e^{-k(z-\eta)}\cos(kx-\omega t) + 2\omega a e^{-z^+}\cos(kx-\omega t-z^+), \tag{2}$$

with $z^+=(z-\eta)/\sqrt{2\nu/\omega}$. Formally, such a profile is linearly defined neglecting the surface elevation (i.e., at z, the altitude from the $z=0$ mean level). This can be generalized with surface-following coordinates [e.g., *Kudryavtsev and Makin*, 2004]. Using here the distance toward the free surface (i.e., $z-\eta$ instead of z) provides a first assessment of the profile with consideration of the linear curvature.

The mean work of the viscous stress W_v ($W_v=\langle \rho_a \nu u_+(z=\eta)\frac{\partial u_+}{\partial z}|_{z=\eta}\rangle$ under laminar conditions) normalized by the power of the underlying wave gives the viscous decay coefficient

$$\mu_v = -\frac{W_v}{C_g\rho_w g a^2/2}. \tag{3}$$

From equation (2), we recover its analytical expression, correcting a factor 2 error in *Collard et al*. [2009, equation (A8)] and *Ardhuin et al*. [2009, equation (5)]

$$\mu_v = -\frac{\omega^2}{gC_g}\frac{\rho_a}{\rho_w}\sqrt{2\nu\omega}. \tag{4}$$

When studying numerically the turbulent atmospheric flow, this expression is expected to produce a low-frequency asymptote, provided that swell steepness and characteristic Reynolds number remain in a valid range for the above hypothesis. Because oceanic swell conditions often exceed the turbulent Reynolds

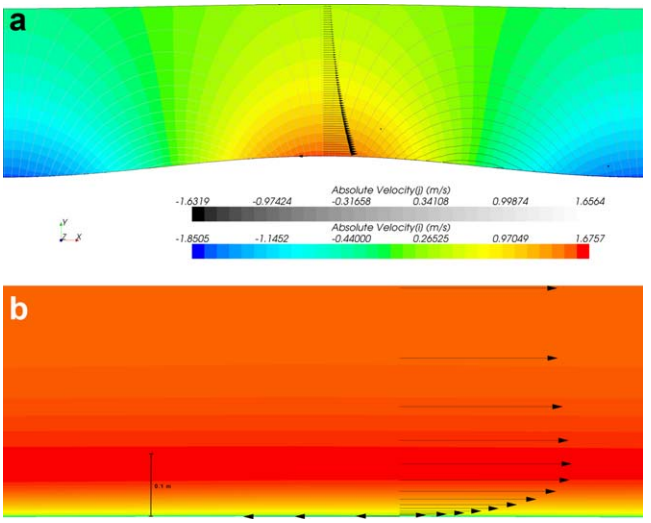

Figure 1. (a) Absolute velocity color map ($\vec{x}$ component) and isolines ($\vec{y}$ component) in the central transect of the fluid atmospheric domain, associated with the vector profile at the wave crest, for the Re$=12\times10^5$ and $T=10$ s test case. (b) Detailed view of the vector profile in the vicinity of the free surface at the crest.

threshold, the characterization of the dissipation coefficient in a large variety of flow regimes still remains to be achieved.

3. Numerical Setup

3.1. Geometry

One of the challenges for the numerical modeling of the atmospheric shear stress above waves is the accurate accounting of the flow in the near free-surface moveable interface. In the most general reference frames, this would require a remeshing process that would definitely be expensive in computation resources and accuracy. In the case of swell however, and more particularly for a unidirectional and monochromatic wave at free surface, the modeling strategy is made quite easier. If the flow is solved in the reference frame attached to the free-surface motion (i.e., phase speed of the monochromatic wave), many commercial CFD software are able to carry such numerical experiments. In the later, the work is performed using the CFD software STAR-CCM+ [*STAR-CCM+*, 2013]. Then, the motion of the reference frame is defined by a linear translation along the $\vec{x}$ direction at a velocity $\vec{U}_{ref}=\vec{C}_{\varphi}$, and the phase of the free-surface elevation is reduced in this frame to a function of space verifying $kx-\omega t=k\left(x_{ref}+C_{\varphi}t\right)-\omega t=kx_{ref}$. Under a hypothesis of strong forcing of the ocean side on the atmospheric boundary layer and a weak retroaction the other way, one can choose to restrain the fluid domain to the atmospheric side, with an appropriate prescribed boundary condition in accordance with the oceanic forcing and motion in the reference frame (Figure 1).

The dimensions of the fluid domain are related to the wavelength λ in the range of ocean swells to consider, with a wavelength of the order of 100 m. The free-surface elevation is periodic in the $\vec{x}$ direction. Our numerical experiments are performed in a domain of length λ. The transverse extension is chosen equal to $\lambda/16$ for practical reasons. An a posteriori sensitivity analysis does not show any influence of the size of this transverse extension, and the width retained still provides a useful length for an output of several realization of the same flow in a turbulent regime, with a manageable mesh size for the largest wavelengths. The mean characteristic vertical extension of the domain is set to $\bar{H}=\lambda/4$, with a top boundary following the streamline expected from linear wave theory

$$H(x_{ref})=\bar{H}+\eta(x_{ref})e^{-k\bar{H}}. \tag{5}$$

This is to be related to the particle displacements at the reference height $z=\lambda/4$, which will enable a proper closure of the streamlines according to the linear potential theory. Both bottom and top boundaries will be imposed with a wall kinetic condition, verifying the wave orbital forcing condition $\vec{u}_{-}=u_{-}\vec{x}+v_{-}\vec{y}$ at the bottom (i.e., linear horizontal and vertical components) and potential solution $\vec{u}_{+}(z=H)$ at the top. Side boundaries, relative to the propagation direction, are defined as symmetric boundary conditions (i.e., normal derivative of a quantity equal to zero at this boundary).

An initial calm condition in the air relative to the absolute frame is easily translated in the reference frame as an initial homogeneous air velocity $-\vec{U}_{ref}$ associated with a mass flow rate input condition at the upwind boundary. The leeward boundary is defined as a flow outlet. For the following experiment, the free-surface maximum is located at the center of our fluid domain along the $\vec{x}$ axis, and we chose a wave propagating in the $-\vec{x}$ direction giving a positive mass flow input at the left-hand side of the domain (i.e., at $x=-\lambda/2$). Boundary conditions are more specifically described in section 4, depending on the stationary or transient properties to be modeled.

Table 1. Characteristic Quantities for $Re = 0.5 \times 10^5$, 5×10^5, and 12×10^5 Simulations, for Four Setup of Different Wave Periods

Re ($\times 10^5$)	T (s)	10.0	12.5	15.0	17.5
	λ (m)	156.13	243.95	351.29	478.15
	Cell number	147,000	427,000	811,000	2,085,000
0.5	a (m)	0.53	0.59	0.65	0.70
	u_- (m s^{-1})	0.33	0.30	0.27	0.25
	ka	0.02	0.01	0.01	0.01
5	a (m)	1.67	1.87	2.04	2.21
	u_- (m s^{-1})	1.24	1.11	1.01	0.94
	ka	0.07	0.05	0.04	0.03
12	a (m)	2.59	2.89	3.17	3.42
	u_- (m s^{-1})	1.62	1.45	1.32	1.22
	ka	0.10	0.07	0.06	0.04

3.2. Solver

The modeling strategy and choice of turbulent closure are related to the nature of the flow to be studied here. For this specific case of viscous shear flow, a Reynolds-Average Navier-Stokes (RANS) approach seems suitable to model the near boundary region at a reasonable computational cost in a domain whose side is related to the wavelength of the free-surface condition. Moreover, in the previously described reference frame, the mean-flow is supposed to reach a steady state, which would permit the use of steady RANS simulations. For an adequate modeling of the shear in the near wall region, a low-Reynolds K-Epsilon [*Lien et al.*, 1996] closure model is retained among other candidate closure models [*STAR-CCM+*, 2013]. The fluid region is modeled as a single component ideal gas material whose density and kinematic viscosity are chosen such as $\rho_a = 1.18\,\mathrm{kg\,m^{-3}}$ and $\nu_a = 1.57 \times 10^{-5}\,\mathrm{m^2 s^{-1}}$. The viscous sublayer needs to be properly accounted in our numerical experiment, and so a low-y^+ wall treatment is used. The mesh is specified accordingly, from a polyhedral grid in the fluid domain to a prism layer refinement in the wall vicinity (bottom and top boundaries). The usual nondimensional distance to the wall $y^+ = \frac{yu^*}{\nu_a}$ (u^* being the reference velocity related to the wall shear stress) is employed as an a posteriori criterion for the validity of the mesh refinement (i.e., $y^+ \sim 1$).

4. Simulations of the Air-Sea Interface

4.1. Homogeneous Domain

A set of simulations is carried out to evaluate the flow properties in an infinite homogeneous type domain. Upwind and leeward boundaries in a 1λ length domain are accordingly connected by a periodic interface. We define a set of 36 numerical experiments with a variation in wave period T in a range of common values (four periods from $T = 10$ s to $T = 17.5$ s) and in Reynolds number (nine values in $5 \times 10^4 \leq \mathrm{Re} \leq 1.2 \times 10^6$) for a characterization of the flow behavior. For a given Reynolds number (e.g., $\mathrm{Re} = 5 \times 10^4$, 5×10^5, and 12×10^5; see Table 1), the steepness of the bottom boundary layer will vary as a function of the wavelength. Thus, the set of experiments will provide an assessment of the proper flow characterization by the Reynolds number previously defined. Steady RANS simulations are carried out up to an order of $O(10^3)$ iterations, and the convergence of the simulations is a posteriori checked considering the residual quantities. The base size for the unstructured grid cells is chosen at 1 m which verifies a convergence test in grid size. The prism layer properties are chosen in order to verify a $y^+ < 1$ property for the higher Re.

Similarly to the characterization of the flat bottom oscillatory flow presented by *Jensen et al.* [1989], the wall shear stress along a wavelength (or equivalently an oscillatory period in their paper) is able to exhibit the laminar to turbulent transition of the shear flow. The near wall region is expected to be the part of the flow exhibiting the greater dependence to the Re. The wall shear stress and its associated work over a moving free surface, in our case, are accordingly sensitive quantities to study for the proper qualification of the flow. When normalizing the work of the total shear stress by the characteristic amplitude of the known Dore expression for the horizontal shear stress (i.e., $a^2\omega^2\sqrt{\omega}$) and plotted in coordinate in the $\overrightarrow{x}$ direction relative to the wavelength, one can recover a proper evaluation of the scalability at any given Reynolds number (Figure 2). The size of the domain and number of cells in the transverse direction to the direction of propagation provides several realizations of the flow along the $\overrightarrow{x}$ direction. While simulations at $\mathrm{Re} = 5 \times 10^4$ and $\mathrm{Re} = 10^5$ show a fairly good agreement with Dore analytical expression of the shear work, the transition toward turbulence observed at $\mathrm{Re} = 2 \times 10^5$ exhibits a strong deviation from the laminar solution over

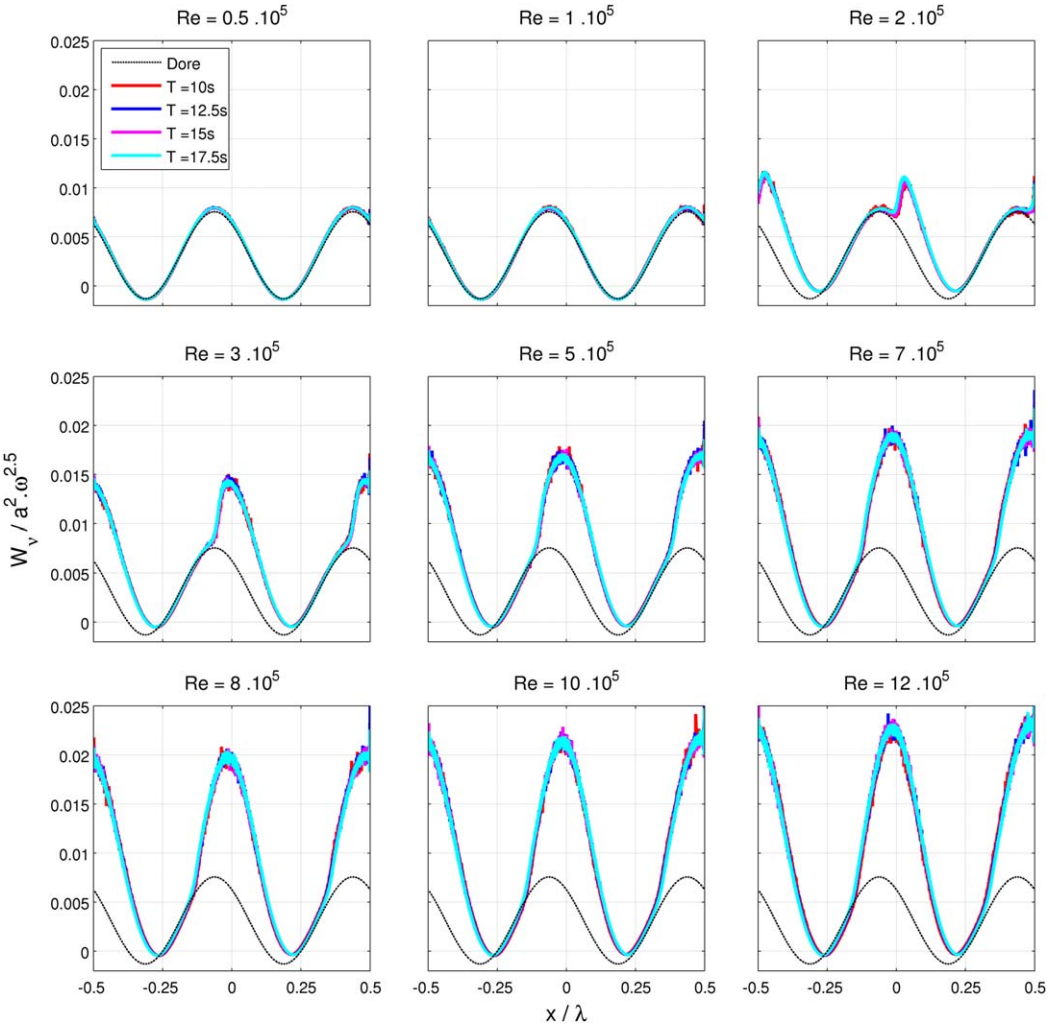

Figure 2. Evolution of the normalized work of the wall shear stress over the free surface against the relative position over a wavelength, from laminar to fully developed turbulent cases for four wave periods (colored lines). The laminar analytical solution is plotted as a reference (black line).

two quarters of the characteristic wave length. This is indeed consistent with *Jensen et al*. observations as well as *Spalart and Baldwin* [1989] direct simulations, for which the transition is initiated between $Re=1.6\times 10^5$ and $Re=2.9\times 10^5$ for the oscillating flat bed case. The turbulent initiation properly occurs in the direct downstream vicinity of the orbital horizontal maximum and influences the shear work all the way to the location where the orbital velocity changes sign. When Re increases, the initiation of the turbulent behavior moves upstream. The development of the transition regime toward a fully developed turbulent one seems as well to be reached for flows at $Re \sim 10^6$. These scaled plots also demonstrate the low-order influence of the steepness over the properties of the turbulent shear. For a given Re, and then for different steepness at each wavelength, the deviation of the shear work remains negligible between wavelengths.

Moreover, the influence of the domain length in such stationary periodic conditions is a posteriori checked with comparisons to longer domains. The results in term of shear work exhibit really low sensitivity to the length of the periodic domain.

4.2. Parameterization of the Decay Rates in Turbulent Regimes

The work of the wall shear stress

$$W_v = \langle \vec{u} \_ \vec{\tau}_v \rangle \tag{6}$$

is averaged over the length of the domain of computation (i.e., 1λ) and normalized by the energy of the underlying wave following equation (3). One recovers from the previous turbulent RANS simulations an

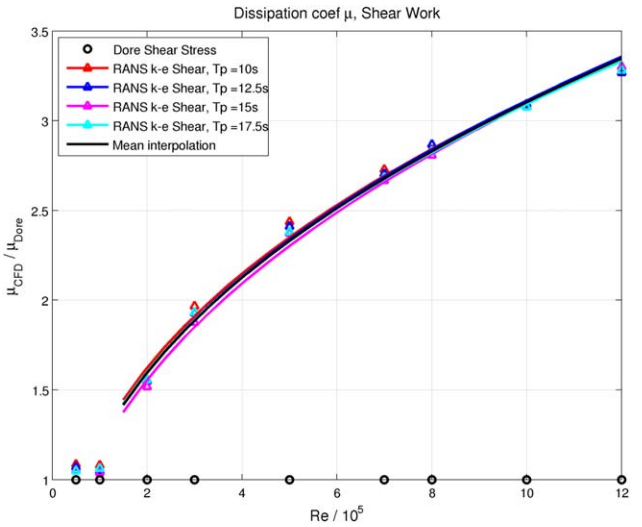

Figure 3. Evolution of the viscous decay coefficient with the associated Reynolds number, relatively to the laminar decay coefficient (markers). Interpolation is performed for the four wave period cases (solid lines)

estimate of the viscous decay coefficients. Their intensity is plotted Figure 3 against the Reynolds value for the test cases previously described.

Both set of laminar simulations at $Re=5\times10^4$ and $Re=10^5$ reflect the previous comments on the work of the shear stress. The deviation in term of decay coefficient shows a slight overestimation in the RANS simulations comprised between 3.8% and 8.4% of Dore coefficients. From the transitory simulations to the fully developed turbulent ones, the computed turbulent decay coefficients deviate as expected from the low *Re* laminar asymptote. The increase in term of ratio to the Dore viscous decay is quantified here. The scaled plot of decay coefficients ratio against Re emphasizes the fairly good agreement between various wave periods. Although *Ardhuin et al.* [2009] assumed that the turbulent shear alone could give a swell decay as large as $56\mu_v$, our computed shear stress can only account for about $3.5\mu_v$. A polynomial regression provides a parametric fit for the four wave period cases. From the set of experiment, the turbulent dissipation rate can be approximated under the form

$$\mu=\begin{cases}\mu_v & ,\mathrm{Re}\ \leq 1.5\times10^5\\ 1.42\mu_v\left(\dfrac{\mathrm{Re}}{1.5\times10^5}\right)^{0.41} & ,\mathrm{Re}\ > 1.5\times10^5.\end{cases} \tag{7}$$

Assuming that the hypotheses considered in this study are valid oceanic and atmospheric conditions, it is clear from this point that the decay related to the turbulent shear stress is not the only mechanism responsible for the observed dissipation rates by *Ardhuin et al.* [2009].

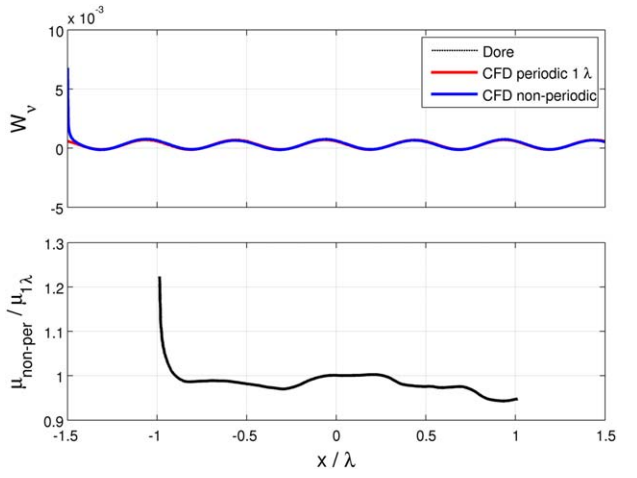

Figure 4. Characterization of the dissipation in transient conditions. (a) Evolution of the work associated with the viscous shear stress in a 3λ nonperiodic domain compared to the 1λ periodic computation, for the $Re=5\times10^4$, $T=10$ s test case. (b) Relative evolution of the associated decay rate per wavelength.

The description of a full realistic airflow above swell, including the coupling between the near wall turbulent sheared flow and an atmospheric circulation is out of scope for the present paper. In that sense, even low-wind conditions include a coupling mechanism between the wave-induced shear and wind shear that required a more detailed analysis in term of numerical modeling and theoretical extension of *Kudryavtsev and Makin* [2004]. However, the same numerical configuration can finally be slightly modified to account for the sensitivity to some of our assumptions.

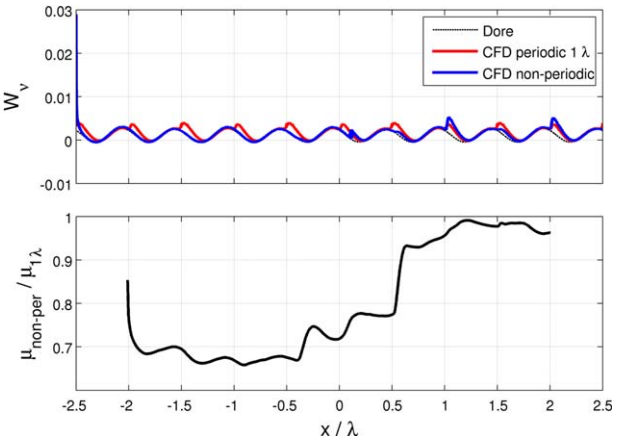

Figure 5. Characterization of the dissipation in transient conditions. (a) Evolution of the work associated with the viscous shear stress in a 5λ nonperiodic domain compared to the 1λ periodic computation, for the Re=12×10^5, T=10 s test case. (b) Relative evolution of the decay rate per wavelength.

4.3. Characterization of the Setup Length

The flow characteristics are evaluated in the previous section under periodic conditions, in order to reproduce a typical setup for a homogeneous infinite medium. We chose here to run steady simulations but without any periodic interface between the mass flow rate upwind boundary condition and the downwind outlet boundary to evaluate the influence of the transient flow over the dissipation rates. So as to characterize a typical setup length for the developed shear flow, the domain is extended to several wavelengths. The atmospheric state is supposed to be at rest at the initial condition (i.e., homogenous $\overrightarrow{u}=-\overrightarrow{U}_{ref}$ in the simulation frame). The tests are performed for the steepest cases of the previous numerical experiments (i.e., T = 10 s), for three characteristic *Re* (laminar Re=5×10^4, transitioning Re=2×10^5, and developed turbulent Re=7×10^5 flows). For the laminar case, a 3λ domain is long enough to emphasize that the typical length for setup remains short compared to the wavelength. Starting form rest, the atmospheric flow is established to the same decay rate μ as the one from a converged periodic configuration in less than a λ/10 length (Figure 4). The increase in dissipation rate reaches 20% for the highest equivalent transient decay coefficient. This pseudo decay rate expressed in space is computed from the same relation as equation (3) as the mean normalized work of the shear stress over a distance λ and expressed at the central location of this rolling mean. For the transitioning case (Figure 5), the turbulent closure requires a 5λ domain to establish a proper convergence toward the periodic solution. Starting from laminar condition on the mass flow rate input, the initiation of turbulence requires a longer length. Still, the dissipation rate over the setup length (about 3λ) is underestimated compared to the periodic dissipation. For the more developed turbulent case (Figure 6), a 3λ domain provides enough space for a proper setup and the turbulence is more easily initiated. The setup length remains negligible as the dissipation rate per wave length is already established at the level of the periodic rate from the start of the domain.

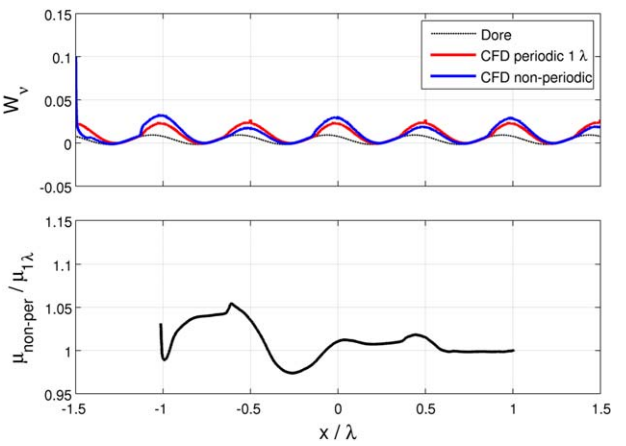

Figure 6. Characterization of the dissipation in transient conditions. (a) Evolution of the work associated with the viscous shear stress in a 3λ nonperiodic domain compared to the 1λ periodic computation, for the Re=7×10^5, T=10 s test case. (b) Relative evolution of the associated decay rate per wavelength.

As long as a full setup from rest is achieved on a short portion of a wavelength with a slight overestimation of the decay rate previously computed from periodic domains for the laminar and turbulent cases, and on about three wave length with a slight underestimation of the decay rates for the transitioning case, the previous periodic computations seem to provide a proper estimation of decay coefficient even for nonstationary wave conditions. As a result, in the case of random waves with a Rayleigh distribution of heights, we may define an

average dissipation rate by considering a succession of monochromatic waves. This will give a gradual transition of the dissipation rate as a function of a significant Reynolds number, similar to what was adapted empirically by *Rascle and Ardhuin* [2013].

5. Discussion and Conclusions

The retroaction of the atmospheric sheared viscous layer driven by swells over the free surface has been simulated with a RANS numerical model. Considering a periodic domain along the wave direction enabled to account for the flow properties under stationary conditions. A set of numerical experiments was conducted for a common range of wave periods and characteristic elevations. Those experiments support the scaling of the atmospheric flow by a Reynolds number similar to the oscillating flat plane boundary layer problem. While work of the shear flow computed under laminar conditions shows a minor deviation from the analytical expression by *Dore* [1978], a transition is characterized by the simulations at a critical Reynolds ($10^5 < \mathrm{Re} < 2\times10^5$) toward the full development of turbulence in the viscous sheared boundary layer. The set of numerical experiment enables to coherently quantify the increase in work when the turbulence is developed over an increasing typical fraction of the wavelength. A parameterization of this increase is deduced in term of viscous decay coefficient computed from the average work of the shear over a wavelength. For the most turbulent case studied, the increase reaches less than $3.5\mu_{Dore}$, corresponding to a measurable *e*-folding decay scale of the order of 20,000 km for oceanic swells. From their observations, *Ardhuin et al*. [2009] were characterizing a swell decay rate up to $56\mu_{Dore}$. Our calculations cannot support such a large value of the dissipation, but we have neglected the effect of the mean wind and thermal effects, and used a smooth sea surface with periodic waves. Also, we did not analyze the work of the pressure field. Indeed, any phase shift from the potential flow theory greatly influences the work related to the pressure stress. This work is not as easily captured as the work of the shear stress and our periodic configuration is not able to provide a reliable quantitative estimate of this mechanism.

We have thus tested the sensitivity of our results to the wave periodicity. Several test cases are conducted to characterize a setup length from initial condition at rest over a wave front. For laminar and turbulent conditions, the setup length for dissipation rate remains short compared to the wavelength and the increase over this length limited. The transitioning case shows a longer setup length but with a lower un-stationary dissipation rate. The un-stationary processes related to the shear stress in an atmospheric flow driven by an underlying swell are finally shown not to depart much from the stationary results.

Other candidate mechanisms for swell dissipation still remain to be investigated to this date. The account of a proper atmospheric circulation and its accurate influence over swell remains a challenge for the numerical modeling tools. For now, the formulation for the increase in turbulent shear stress proposed here would not be able by itself to set a proper source term related to swell dissipation in operational wave models, but it is expected to help in clarifying the magnitude of respective dissipation mechanisms in the swell energy balance.

Acknowledgments
The work presented here was supported by LHEEA at Ecole Centrale de Nantes, France, in the context of the scientific gathering LabexMer (Program "Investment for the future," grant ANR-10-LABX-19-01). The authors thank the anonymous reviewers for their valuable comments and suggestions to improve this manuscript.

References

Ardhuin, F., B. Chapron, and F. Collard (2009), Observation of swell dissipation across oceans, *Geophys. Res. Lett.*, *36*, L06607, doi:10.1029/2008GL037030.

Collard, F., F. Ardhuin, and B. Chapron (2009), Routine monitoring and analysis of ocean swell fields using a spaceborn SAR, *J. Geophys. Res.*, *114*, C07023, doi:10.1029/2008JC005215.

Dore, B. D. (1978), Some effects of the air-water interface on gravity waves, *Geophys. Astrophys. Fluid Dyn.*, *10*, 215–230.

Gundogdu, M., and M. Carpinlioglu (1999a), Present state of art on pulsatile flow theory. Part 1: Laminar and transitional flow regimes, *JSME Int. J.*, *42*(3), 384–397.

Gundogdu, M., and M. Carpinlioglu (1999b), Present state of art on pulsatile flow theory. Part 2: Turbulent flow regime, *JSME Int. J.*, *42*(3), 398–410.

Guo, X., and L. Shen (2013), Numerical study of the effect of surface wave on turbulence underneath. Part 1. Mean flow and turbulence vorticity, *J. Fluid Mech.*, *733*, 558–587.

Harris, D. L. (1966), The wave driven wind, *J. Atmos. Sci.*, *23*(6), 688–693.

Jensen, B., B. Sumer, and J. Fredsøe (1989), Turbulent oscillatory boundary layer at high Reynolds numbers, *J. Fluid Mech.*, *206*, 265–297.

Kudryavtsev, V. N., and V. K. Makin (2004), Impact of swell on the marine atmospheric boundary layer, *J. Phys. Oceanogr.*, *34*, 934–949.

Lien, F., W. Chen, and M. Leschziner (1996), Low-Reynolds-number eddy-viscosity modelling based on non-lineard stress-strain/vorticity relations, in *Proceedings of the 3rd Symposium on Engineering Turbulence Modelling and Measurements*, edited by W. Rodu and E. Bergeles, pp. 91–100, Elsevier, Amsterdam, N. Y.

Phillips, O. (1961), A note on the turbulence generated by gravity waves, *J. Geophys. Res.*, *66*(9), 2889–2893.

Rascle, N., and F. Ardhuin (2013), A global wave parameter database for geophysical applications. Part 2: Model validation with improved source term parameterization, *Ocean Model.*, *70*, 174–188.

Spalart, P., and B. Baldwin (1989), Direct simulation of a turbulent oscillating boundary layer, *Turbul. Shear Flows*, *6*, 417–440.

STAR-CCM+ (2013), *STAR-CCM+ 8.02 User Manual*, CD-ADAPCO, Melville, N. Y.

Weber, J. (1983), Measurements of the wind-wave energy flux in an opposing wind, *J. Fluid Mech.*, *137*, 115–129.

Young, I., and R. Sobey (1985), Measurements of the wind-wave energy flux in an opposing wind, *J. Fluid Mech.*, *151*, 427–442.